Mon. Not. R. astr. Soc. (1990) **243**, 713–720

Simultaneous multifrequency observations of the Seyfert 1 galaxy NGC 4051: constant optical–infrared emission observed during large-amplitude X-ray variability

C. Done[1,†], M. J. Ward[1,7], A. C. Fabian[1], H. Kunieda[2], S. Tsuruta[3], A. Lawrence[4], M. G. Smith[5] and W. Wamsteker[6]★

[1] *Institute of Astronomy, Madingley Road, Cambridge CB3 0HA*
[2] *Department of Astrophysics, Nagoya University, Japan*
[3] *Department of Physics, Montana State University, Bozeman, MT 59717, USA*
[4] *School of Mathematical Sciences, Queen Mary and Westfield College, Mile End Road, London E1 4NS*
[5] *Joint Astronomy Center, 665 Komohana Street, Hilo, HI 96720, USA*
[6] IUE *Observatory, European Space Agency, Apartado 54065, 28080 Madrid, Spain*
[7] *Royal Greenwich Observatory, Madingley Road, Cambridge CB3 0EZ*

Accepted 1989 October 25. Received 1989 October 23; in original form 1989 September 25

SUMMARY

We report simultaneous infrared, optical, ultraviolet and X-ray observations of the low-luminosity Seyfert 1 galaxy, NGC 4051. A new method of reduction was developed to correct the optical flux for atmospheric variations due to seeing and extinction. The X-ray flux varied by factors of up to 2 on time-scales of tens of minutes whilst the optical flux remained steady to within 1 per cent. Our results rule out all models, including Compton scattering and synchrotron models, in which a single electron population is responsible for the formation of both the infrared-to-optical and the X-ray spectra. The optical emission region must be an order of magnitude larger than, or completely separate from, the X-ray source.

1 INTRODUCTION

The spectrum of a typical active galactic nucleus (AGN) emits roughly equal power per decade of frequency from the far-infrared (IR) to X-ray frequencies. This power is either spread over the whole energy range by the primary emission process of the central engine, or is re-processed and re-distributed by secondary mechanisms at some distance from the source. If the broad spectral energy distribution is due to the primary process, then variability at different frequencies is likely to be correlated. Rapid variations, of the order of the light crossing-time of the source, are important here, since slow changes could be due to an overall modulation in the rate of energy generation in the nucleus, which would be expected eventually to affect the whole spectrum.

We present the results of a search for correlated, rapid, X-ray and optical variability in the Seyfert 1 galaxy, NGC 4051. This is the first such study of a Seyfert-type AGN. Earlier multifrequency work concentrated on BL Lac and OVV objects (see e.g. Makino *et al.* 1987 and references therein). A search for rapid optical variability in NGC 4151 by Lawrence *et al.* (1981) produced a null result, but the lack of simultaneous X-ray data restricted the conclusions that could be drawn.

We chose to study NGC 4051 as, unlike NGC 4151, it is highly variable in X-rays on all time-scales down to the minimum observable of 100 s (Lawrence *et al.* 1987; Matsuoka *et al.* 1989). It is also known to be strongly variable in the Hβ emission line (Peterson, Crenshaw & Meyers 1985) on a time-scale of a year, and there is marginal evidence for optical continuum variability on a level of 20–30 per cent (Lyutyi 1977; Penston *et al.* 1974). A further advantage of this object is that its spectral energy distribution shows no upturn in the optical/UV spectrum (Edelson & Malkan 1986), unlike the PG Quasars, reported by Sanders *et al.* (1989). Any accretion disc spectrum must therefore contribute only at higher energies, in the EUV and soft X-ray region. Thermal dust emission is unlikely to contribute at wavelengths higher than 1 μm, so the observed optical spectrum is not contaminated by either of these components.

The galaxy was observed with the *GINGA* X-ray satellite and the resulting X-ray light curve compared with the optical light curve obtained from repeated *B*-band CCD images of a field containing the galaxy and a star of comparable brightness. As detailed in Section 2, variations in the apparent brightness of the field star were used to correct the brightness of the nucleus of NGC 4051 for atmospheric seeing and extinction changes so that the intrinsic light curve of the

★ Affiliated to the Astrophysics Division, Space Sciences Department.
†Present address: Goddard Space Flight Center Greenbelt, MD 20771, USA.

nucleus could be obtained. No rapid optical variations were found although the X-ray flux was continuously changing by up to a factor of 2.

The galaxy was also observed in the IR with the UKIRT facility. No evidence for variability was seen in the IR light curve, further strengthening the case for different variability behaviour in the high- and low-energy spectra. These data, together with a UV spectrum from *IUE*, gave a snapshot of the spectral energy distribution, which confirmed the absence of the 'big blue bump' at optical/UV energies.

We discuss the implications of the lack of any correlated rapid variability for models of the continuum emission of AGN. Simple models in which the IR–optical and the X-ray continua are produced by the same electron population are ruled out. We show that the X-ray and optical continua probably originate in distinct spatial regions which must either be separate from each other, or be of very different sizes.

2 THE OBSERVATIONS

NGC 4051 was observed in 2–20 keV X-rays by *GINGA* on 1988 May 13 to 15. Simultaneous observations were made at longer wavelengths with the *IUE* satellite, the Jacobus Kapteyn Telescope (JKT) on La Palma, and the United Kingdom Infrared Telescope (UKIRT) in Hawaii. A log of the observations is given in Table 1.

2.1 Optical

Observations were made in the *B*, *U* and *I* bands with a blue-sensitive CCD at the Cassegrain focus of the 1-m JKT. Both the nucleus of NGC 4051 and one field star of comparable brightness were included in each image. In the *B* and *I* bands, the comparison star used was 'Star 2' in Penston, Penston & Sandage (1971), whereas in *U* the brighter 'Star 1' was a better match to the nuclear flux. Integration times of 100–600 s were used over six clear nights (see Table 1).

Our major aim is to obtain relative photometry of the nucleus of NGC 4051 over the interval that *GINGA* was observing the source. The field star is used to correct for atmospheric effects. The seeing was typically 1–2 arcsec. By trial and error we found that measurement of the flux within a 6 arcsec diameter collects most of the flux from the star or nucleus whilst reducing the dilution of the nucleus by light from the rest of the galaxy. Direct division of the flux of the nucleus by the flux of the star removes the large-scale variations due to changes in atmospheric conditions. However, the star and nucleus have different spectra and so are affected by extinction in a slightly different manner. Also, the extended profile of the host galaxy has a different response to changes in seeing than the unresolved stellar profile. These small-scale atmospheric effects are not removed by a simple flux division.

We instead carry out a more detailed analysis in which the gross extinction changes, which vary as the cosine of the zenith distance of the object, are first removed from the star and nucleus. The detailed seeing changes in the nucleus are then eliminated by using a scaled template of the stellar variations. This approach reduces the scatter in a constant light curve to a value close to that expected from Poisson counting statistics.

The number of counts within a 6-arcsec aperture centred on the galaxy nucleus and star were measured from the CCD images after standard bias-subtraction and flat-fielding had been carried out. The results from the night of 1988 May 18–19 are shown in Fig. 1. The decrease in the flux with zenith distance, z, has the expected functional form

$$\log(f/f_0) = -0.4A/\cos z, \tag{2.1}$$

where f is the observed flux, f_0 is the flux above the atmosphere and A is the extinction in mag per unit air mass (determined separately for both the star and galaxy). The best-fit extinction curves for the star and galaxy are shown overlaid on the data in Fig. 1.

Table 1. Log of observations of NGC 4051.

Date (UT)	Instrument	Integration Time (s)	Flux (erg s^{-1} cm^{-2} Hz^{-1})	σ/I (per cent)
88 May 13 21:52 – 14 11:43	GINGA	256	1.56×10^{-11} (2.3–8.7 keV) †	77
88 May 14 22:55 – 15 10:08	GINGA	256	1.98×10^{-11} (2.3–8.7 keV) †	54
88 May 15 22:58 – 16 13:24	GINGA	256	1.63×10^{-11} (2.3–8.7 keV) †	71
88 May 15 01:49 – 06:49	IUE (SWP33531)	18000	7.50×10^{-27} (1500 Å)	...
88 May 14 23:50 – 15 01:40	IUE (LWP13231)	6600	3.13×10^{-26} (2500 Å)	...
88 May 12 23:10 – 13 00:52	JKT (U)	600	6.12×10^{-26}	0.36
88 May 17 00:14 – 02:01	JKT (U)	600	6.69×10^{-26}	0.64
88 May 13 01:23 – 03:06	JKT (B)	600	9.36×10^{-26}	0.12
88 May 14 21:13 – 15 04:29	JKT (B)	600, 300	9.54×10^{-26}	0.35
88 May 15 20:58 – 16 03:49	JKT (B)	300	9.60×10^{-26}	0.76
88 May 16 22:13 – 23:10	JKT (B)	300	9.60×10^{-26}	0.45
88 May 17 21:09 – 23:33	JKT (B)	300	9.66×10^{-26}	0.69
88 May 18 21:15 – 19 00:50	JKT (B)	300, 100	9.34×10^{-26}	0.50
88 May 13 04:20 – 04:54	JKT (I)	300	24.5×10^{-26}	0.45
88 May 14 06:43 – 06:48	UKIRT (J)	300	48.9×10^{-26}	...
88 May 16 08:53 – 08:58	UKIRT (J)	300	40.3×10^{-26}	...
88 May 14 06:48 – 06:53	UKIRT (H)	300	65.7×10^{-26}	...
88 May 16 08:58 – 09:03	UKIRT (H)	300	63.3×10^{-26}	...
88 May 14 06:55 – 08:06	UKIRT (K)	300	74.3×10^{-26}	5.7
88 May 15 08:21 – 10:22	UKIRT (K)	300	71.9×10^{-26}	2.6
88 May 16 09:03 – 10:59	UKIRT (K)	300	71.4×10^{-26}	2.5

†Flux conversion of 2.25×10^{-12} erg cm^{-2} s^{-1} Hz^{-1} = 1 count s^{-1} in the 2.3–8.7 keV band.

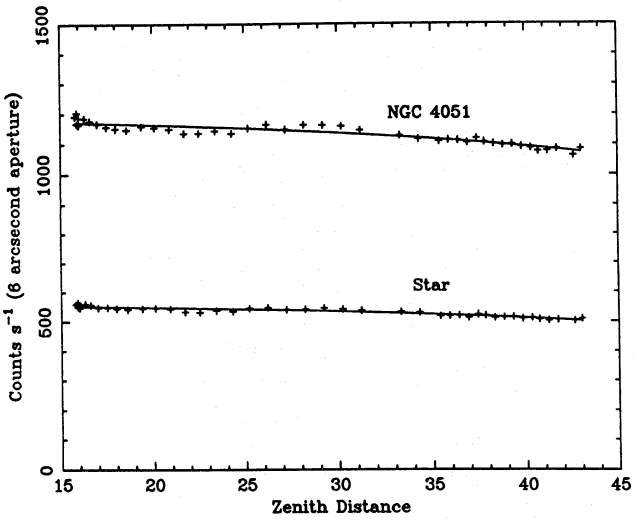

Figure 1. The flux (in counts s^{-1}) in B of the star and galaxy on 1988 May 18–19. The Poisson error associated with the data is much smaller than the symbol used to mark the points. The increase in extinction with zenith distance is clearly seen. The solid lines are the best-fitting extinction curves as in equation (2.1). Residual variations about these curves are correlated, e.g. at a zenith distance of 22 degrees, both the stellar and galactic fluxes lie below the curve. Changes in microscale extinction or in the seeing are responsible for these variations.

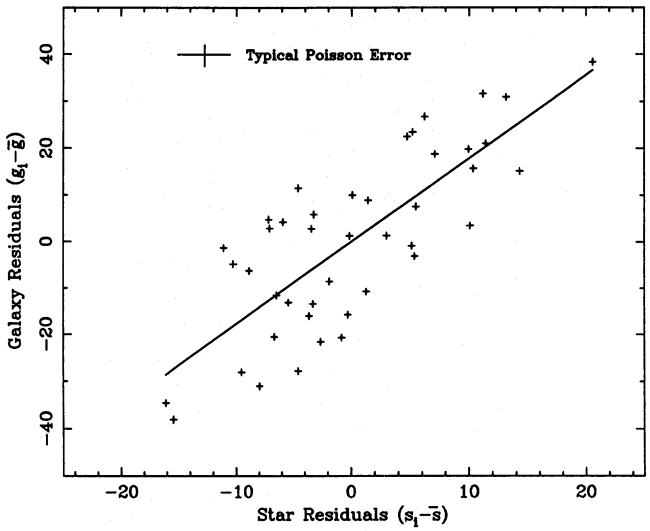

Figure 2. The residuals about the mean, extinction-corrected flux for the star and the galaxy. The correlation indicates that the variability is produced by atmospheric effects. If the seeing affected both star and galaxy equally, then the best-fit straight line should have an index equal to the ratio of the galactic and stellar fluxes. Instead, the line has a slope of 1.8, whereas $\bar{g}/\bar{s} \sim 2.1$. The blurring of the extended host galaxy profile means that seeing changes have less of an effect on the aperture photometry than for the star.

There are two nights (1988 May 16–17, 17–18) where there are insufficient data to determine the extinction parameters. The range in zenith distance is too small to show a noticeable trend, so the data were not corrected for extinction.

The residual variations in the galaxy and star are still correlated because of rapid seeing changes and microscale extinction variations (see Fig. 2). The fractional change in the flux from the galaxy is less than that of the star. The effect of changes in the seeing is diminished because photons from the extended host galaxy profile are scattered into the central 6 arcsec aperture. In the example shown in Fig. 2, the fractional amplitude of the galactic flux variations are only 85 per cent as large as those in the star.

The starlight residuals about the mean form a template that we scale in amplitude and compare to the AGN residuals. The template is defined by

$$r_i = s_i - \bar{s}, \tag{2.2}$$

where r_i are the residuals of the stellar flux s_i around the mean, $\bar{s}$. We use this to form an estimate of the flux from the nucleus, g_i', defined by

$$g_i' = \bar{g} + Gr_i, \tag{2.3}$$

where $\bar{g}$ is the mean galaxy flux, and G is a free parameter that determines the relative amplitude of the stellar and nuclear variations. Both these parameters are found by minimizing the difference between the predicted and actual fluxes. The fit is shown on the galaxy light curve in Fig. 3.

The seeing variations are then subtracted from the fluxes for the nucleus of NGC 4051 to produce the final light curves in Fig. 4, which are scaled to the extinction-corrected stellar mean for each night. The flux and root mean square variability, σ/I, for each night are given in Table 1. The variability is now significantly below 1 per cent, an improvement of up to a factor of 4 over the variability limits obtained by a straightforward division of the galaxy and stellar fluxes. The figures are very close to the errors expected purely from counting statistics, indicating that the star does not undergo any intrinsic rapid changes which would, of course, invalidate our analysis.

The total variability in B over the six nights of observation was $\sigma/I = 1.4$ per cent. This increased scatter is due to the errors in determining the extinction coefficient for each

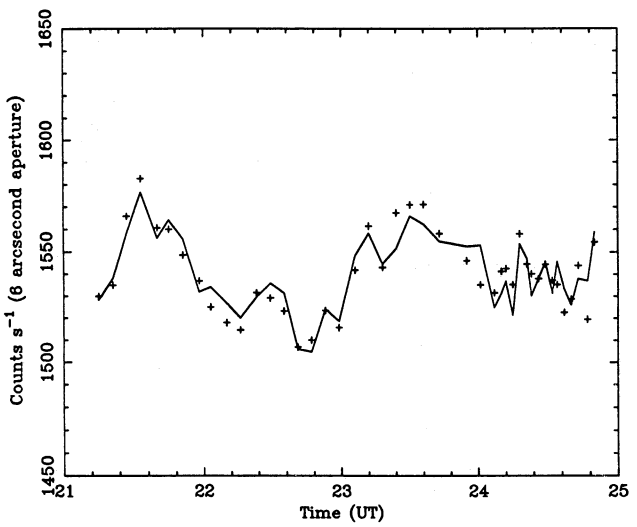

Figure 3. The galactic flux, corrected for extinction as in Fig. 1. Note the false zero used to emphasize the residual variations. The solid line is the template stellar flux. The amplitude of the stellar residuals about its extinction-corrected mean level has been changed until the best match to the galaxy residuals is found. The excellent fit emphasizes the correlated variability due to changing atmospheric conditions.

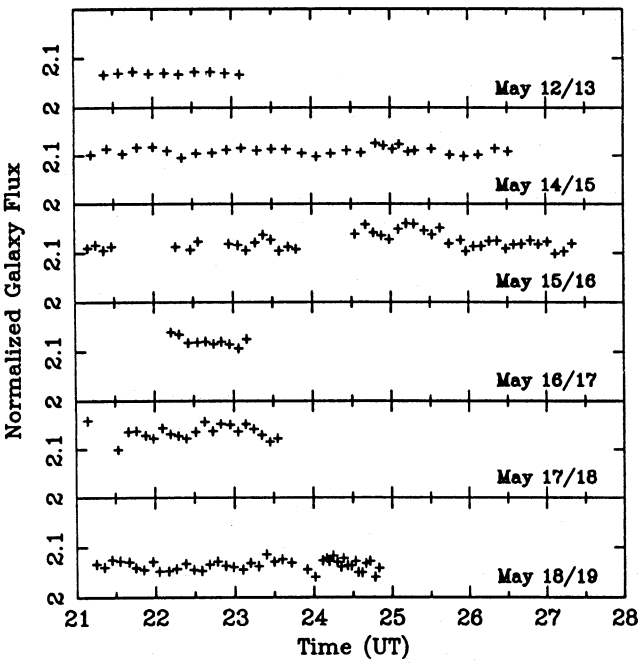

Figure 4. The galactic flux in *B* after removal of extinction and seeing variations. The data from all six clear nights are shown. The extinction-corrected mean stellar flux is used to normalize the data. The residual variability in the light curves is less than 1 per cent. Note the false zero used on the flux axis.

night. The fluxes from night to night differ by at most a few per cent, but the errors within a particular night are considerably better. This is even more marked in *U*, where there is a variation of 4.6 per cent between the two nights on which the *U* images were taken. The extinction errors in *U* are larger than in *B*, leading to a greater discrepancy between separate light curves. The mean flux and variability in each band is given in Table 2.

Our procedure enables us to derive strong limits to the amount of optical variability of an object by removing the effects of atmospheric variations from the light curve using a comparison star in the same field. This technique is particularly useful in searching for short time-scale (<few hours) variability, but is less reliable for systematic, low-amplitude (<few per cent) trends throughout the night as these can be confused with the effects of extinction.

2.2 X-ray observations

NGC 4051 was observed with the large-area proportional counter (LAC) on *GINGA* from 1988 May 13–16, followed by a background observation on 1988 May 17. This detector is the most sensitive instrument over the 2–20 keV energy range flown to date (for details see Turner *et al.*, in preparation). It can resolve a factor of 2 change in a 2–20 keV flux of 2×10^{-11} erg s^{-1} cm^{-2}, similar to that of NGC 4051, on time-scales as short as 300 s. The instrument is ideally suited to a search for rapid (time-scales of minutes) variability, but the low earth orbit means that the observation is interrupted after 20–40 min by periods of high background from radiation belts and by earth occultations. These breaks in the light curve make variability harder to quantify on time-scales of hours.

Accurate background subtraction is essential as the source is faint (~1 mCrab). The high-energy, particle-induced, background in the detector is monitored throughout the observations. It is used to model the total background level using the data collected during the off-source background observations.

Only data from periods of low background were used to form the light curves and spectrum. After a careful examination, some data from the mid-layer detectors were included in the analysis to improve the source statistics, the selection criteria being consistency of the time-dependent behaviour between data in the two layers.

The resultant light curves in the soft (2.3–8.7 keV) and hard (8.7–20.9 keV) bands are shown in Fig. 5. There is continual variability over the whole observation down to the smallest resolvable time-scales of a few hundred seconds.

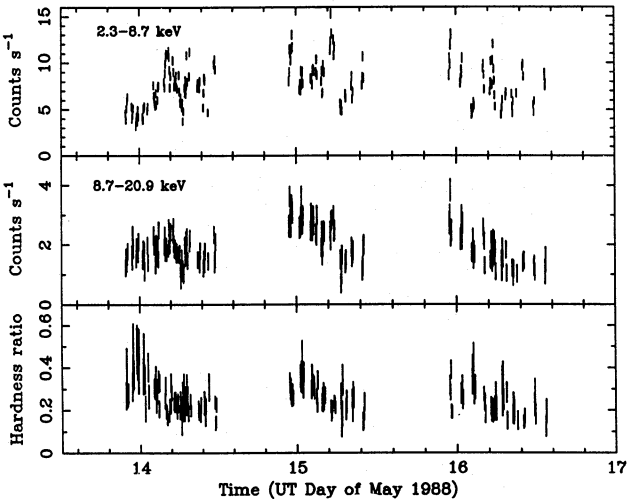

Figure 5. The soft (2.3–8.7 keV) and hard (8.7–20.9 keV) X-ray light curves as measured by the *GINGA* satellite. The hardness ratio is defined as the ratio of the count rates in the two bands (hard/soft). This decreases as the soft X-ray flux increases, indicating a steepening of the spectrum as the source brightens.

Table 2. All figures are given in erg cm^{-2} s^{-1} Hz^{-1} and are dereddened assuming $E(B-V)=0.08$. Variability (σ/I) is quoted as a percentage.

Filter	Mean Flux	Mean σ/I	Galactic Stellar Flux	Dereddened Nuclear Flux	Nuclear variability (σ/I)
U	6.40×10^{-26}	0.50	8.96×10^{-27}	8.03×10^{-26}	0.58
B	9.52×10^{-26}	0.48	3.14×10^{-26}	8.65×10^{-26}	0.71
I	24.5×10^{-26}	0.45	9.07×10^{-26}	17.2×10^{-26}	0.71
J	40.3×10^{-26}	...	19.4×10^{-26}	22.5×10^{-26}	...
H	63.3×10^{-26}	...	24.8×10^{-26}	40.3×10^{-26}	...
K	72.4×10^{-26}	3.9	19.4×10^{-26}	54.4×10^{-26}	5.3

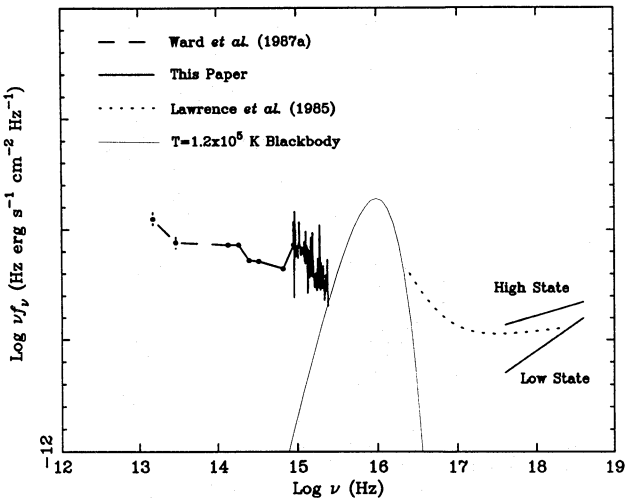

Figure 6. The multifrequency spectrum. Heavy lines indicate data given in this paper. The dotted line is the two power-law fit to the *EXOSAT* low energy (LE) data of Lawrence *et al.* (1985). The maximum blackbody spectrum in the EUV which is consistent with both the *IUE* and the LE data has a temperature of 1.2×10^5 K and is plotted as a thin line. As discussed in Section 4.2, the difference in power between the photon source and scattered spectrum will be the same in the IR as in the EUV. The varying electron population responsible for the X-ray spectrum scatters IR photons into a power-law spectrum that starts a factor of ~ 12 (low state) below the IR flux (the same factor by which the soft X-ray spectrum lies below the EUV bump). In the decade between the IR and optical (B) band, the scattered spectrum rises (in νf_ν) as it has the same index as the X-ray power law. This maximum EUV power gives a minimum in the IR scattered flux which is around 8 per cent of the optical B band flux, i.e. easily detectable.

The hardness ratio between the two bands also varies, in the sense that the spectrum is harder at lower luminosities. This is similar to previous observations reported by Lawrence *et al.* (1985) and Matsuoka *et al.* (1989).

The spectrum was modelled by a power-law continuum and a 6.4 keV fluorescence line, together with absorption by a galactic column of neutral atoms along the line-of-sight of 1.1×10^{20} atoms cm^{-2}. A more detailed analysis suggesting that a higher column may be more applicable to the spectrum is discussed by Kunieda *et al.*, in preparation. We show the best-fit unabsorbed spectra in a high and low luminosity state in Fig. 6. These are given by $f_\nu = 2.74 \times 10^{-15}\ \nu^{-0.79}$ and $1.20 \times 10^{-20}\ \nu^{-0.51}$ erg s^{-1} cm^{-2} Hz^{-1}, respectively.

2.3 Infrared

We observed NGC 4051 on the nights of 1988 May 14–16 with the infrared camera (IRCAM) on UKIRT. The 37×35 arcsec field of view of this InSb imaging array is smaller than the optical CCD field, so it was not possible to include a comparison star in the frame. Instead, standard stars were observed at frequent intervals between the observations of NGC 4051. Without a simultaneous estimate of the extinction and seeing, the scatter in the data is larger than that in the optical light curve. Nevertheless, the flux is constant to within 4 per cent in the 25 images taken over the three nights at K. Spot measurements at J and H for the overall snapshot of the spectral energy distribution were also taken, and details of the observations for each night are given in Table 1.

The counts within a 6-arcsec aperture were measured after standard dark current and sky subtraction procedures were carried out on the 20×15 s exposures and the data were corrected for atmospheric extinction. An analysis of the standard stars showed that the nights of 1988 May 15–16 and 16–17 were photometric to within 2–3 per cent. There are not enough standard star observations on the night of 1988 May 14–15 to determine whether the 20 per cent decrease in J between this night and that of 1988 May 16–17 is due to seeing changes or intrinsic variability. We believe that seeing changes are responsible, since the observations at H and K agree with those taken on 1988 May 16–17. It is unlikely that intrinsic source variability is present only at 1.2 μm. Poor photometric conditions also explain the increased scatter in the K light curve on the night of 1988 May 14–15. Even including the data from this night, the total variability in the K light curve over the three nights is less than 4 per cent (see Table 2 for the mean flux and variability).

2.4 Ultraviolet

The *IUE* spectra were used only to get a snapshot of the flux distribution, rather than to monitor for variability because of the long integration times required to get a well-exposed spectrum. Both short and long wavelength spectra, SWP33531 and LWP13231, were taken and the data extracted as appropriate for a faint source. Details of the observations are shown in Table 1.

3 THE SPECTRUM

The simultaneous IR, optical (I, B and U), UV and X-ray observations form a snapshot of the spectral energy distribution. This is corrected for the effects of reddening and the stellar contribution is subtracted, to leave the instantaneous nuclear spectrum shown in Fig. 6.

The host galaxy is clearly visible in the optical CCD frames, implying a significant contribution from the starlight even in small apertures. This is also important in the near IR. We used the CCD images to estimate the amount of stellar contamination in each band, as described by Malkan & Filippenko (1983). The cumulative stellar profile is matched to the inner part of the galaxy profile. This gives the contribution from the unresolved nuclear component at each radius. The fraction of resolved starlight to the total flux in a 6-arcsec aperture is 0.14, 0.33 and 0.37 in the U, B and I bands, respectively. The conclusion that a large fraction of the optical continuum is not due to starlight is supported by the relatively weak absorption (Malkan & Filippenko 1983) in lines which are known to be good indicators of the stellar population, such as the Mg Ib triplet (λ5167, λ5173, λ5184).

The lack of any comparison star within the field of the IR detectors means that the cumulative profile technique cannot be used. Instead, the stellar fluxes in the U and B bands are used to deduce the stellar fluxes at J, H and K, assuming the spiral galaxy colours given by Ward *et al.* (1987b). The stellar fluxes can be compared to the observed flux, to give the fraction of starlight to total flux in the aperture. These are 0.48, 0.39 and 0.27 in the J, H and K bands, respectively.

The limits on variability depend on the fraction of nuclear to stellar flux, since starlight contamination is a constant

component which dilutes any continuum variability. Limits on the rapid *nuclear* variability are given in Table 2.

The small 2200 Å dust absorption feature in the UV spectrum is consistent with the published intrinsic reddening of $E(B-V)=0.08$ (Edelson & Malkan 1986). A standard Milky Way reddening curve was used to correct the IR (Savage & Mathis 1979, scaled up to $R=3.2$), optical and UV (Seaton 1979) data. Stellar subtracted and dereddened fluxes are given in Table 2.

The IR and optical points define a continuum power law given by $f_\nu = 6.19\times10^{-7}\ \nu^{-1.28}$ erg s^{-1} cm^{-2} Hz^{-1}. This is flatter than the power-law continuum fitted by Edelson & Malkan (1986). They included the *IRAS* points, which at 60 and 100 μm are contaminated by emission from the underlying galaxy (Ward *et al.* 1987a). Ignoring these two points, their data give a very similar spectrum, indicating that source variability in the IR/optical is small on time-scales of years. We show the 10 and 20 μm small aperture fluxes given in (Ward *et al.* 1987a) in Fig. 6. Although these are not simultaneous, the lack of IR variability means that these give a good indication of the IR spectrum at lower energies. The points are in agreement with the optical/IR power law deduced from our data.

4 DISCUSSION

We now consider what constraints can be obtained from the lack of correlated variability. As a specific limit on the variability, we note that on May 15, at around 2230 UT, the X-ray flux increased by 50 per cent over about 1500 s (Fig. 7). Over that interval, no change exceeding 0.7 per cent was observed in the *B* band, corresponding to a maximum change in the nucleus of less than 1 per cent. (Similar, although not simultaneous, limits are obtained in the *U* and *I* bands.) We therefore assume that there is a factor of at least 50 between the variability amplitude in the X-ray and optical. We also assume that the X-ray and infrared-to-optical continua are characterized by power-laws of energy indices of 0.51 and 1.28, respectively. The infrared-to-optical power law extends to frequencies lower than the *B* band by a factor of at least 50. The varying X-ray spectrum is assumed to extend down to at least 0.2 keV from the *EXOSAT* work of Lawrence *et al.* (1987) and Turner & Pounds (1989). Both bands separately cover almost two decades of frequency (Fig. 6).

Consider that there is a single emission region for both spectral bands. Unless special geometry or relativistic beaming is involved, the region must be smaller than 1500 lightseconds during our observations and, if of the same size as during previous more rapid changes, less than a few hundred lightseconds.

The different spectral shapes of the optical-to-infrared and X-ray continua and the different variability behaviour of the bands suggest that we are dealing with different emission regions, but the possibility of a single emission region is investigated in detail in the following sections.

4.1 Single electron population

If the X-ray variability is due to the emitting electrons varying in number or energy, then those same electrons cannot produce much radiation in the optical either by direct emission or by upscattering IR photons to optical frequencies. This rules out models in which the same electron population is used to make both the IR/optical and X-ray spectra, such as synchrotron-self-Compton (SSC) spectra. Such models can reproduce the different spectral indices in the IR/optical and X-ray bands (Zdziarski 1986), but generally predict correlated variability in the two bands. There is one special case in which SSC models can produce a constant IR/optical spectrum with a simultaneously varying X-ray spectrum (Ghisellini, George & Done 1989), but this requires that the energy density in the magnetic field dominates that in the radiation field. Under these conditions, the luminosity in the Compton scattered X-ray spectrum is much less than that in the IR/optical synchrotron spectrum. This model is ruled out as there is about the same amount of power in the X-ray and IR/optical spectra (see Fig. 6).

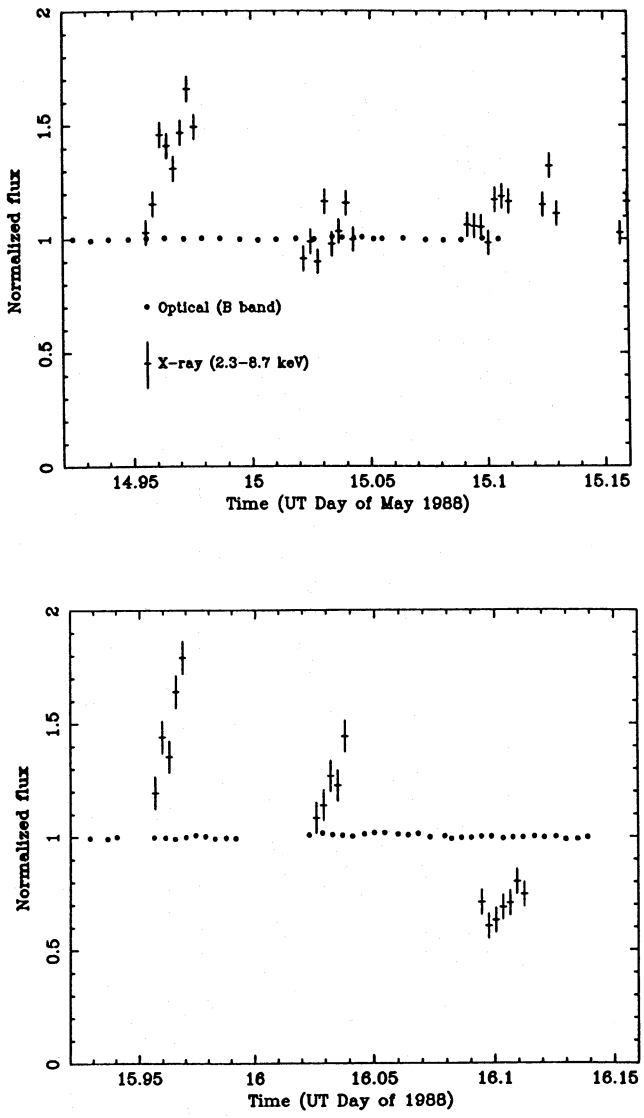

Figure 7. Simultaneous variability on 1988 May 14–15 and 15–16. The normalized light curves show the large-amplitude X-ray variability and constant optical (*B*) flux. The size of the points marking the optical data roughly indicates the size of the 1σ error bars.

No single electron population can reproduce the observed variability and spectrum. Relaxing the assumption of a single distribution, we now consider whether the IR/optical and X-ray emission can arise from the same spatial region, irrespective of how they are each produced.

4.2 X-rays produced by an electron distribution with $\gamma < 30$

4.2.1 *Varying electron population*

First, let us assume that the observed X-ray 2–20 keV spectrum is produced by scattering seed photons in the EUV region and that the electron population produces no direct radiation in the IR/optical band. The seed photons are unlikely to be cyclotron in origin, as this requires a large magnetic field ($B > 10^9$ G). The X-rays are thermal or relativistic Compton-scattered EUV photons. Thermal models require an electron temperature greater than 20 keV so that the X-ray spectrum extends out to at least this energy. For a relativistic electron distribution we require that the power-law electron population continues up to Lorentz factors, $\gamma \sim 30$, in order that the boosted EUV photons, at frequencies $\sim 10^{16}$ Hz, can produce a spectrum extending to 10^{19} Hz (20 keV). In either of these cases, the electrons also produce a Compton-scattered component in the optical *B* band from infrared photons (at a frequency $\sim \gamma^2$ times less than the optical). This component will have the same amplitude as the X-ray variability and would thereby have been easily seen. To quantify this we note that the fraction of the energy emitted by energetic electrons in the optical to that in the X-ray band is approximately equal to the ratio of the energy densities of the infrared photons to the EUV photons. The EUV emission is probably dominated by thermal emission from an accretion disc, as found in many other Seyfert 1 galaxies (e.g. Arnaud *et al.* 1985). The largest *blackbody* EUV bump that is consistent with the observed *IUE* and X-ray spectra is shown in Fig. 6. The *EXOSAT* data indeed indicate that there is a bump present at about this level (Lawrence *et al.* 1985). (In practice the bump will be broader and flatter than a single-temperature blackbody and so lower than shown in the figure, thereby strengthening our conclusions. It is most unlikely to make any significant contribution in the *B* band as the optical/UV spectrum in Fig. 6 is falling rather than rising.) It means that the energy density in the IR/optical band is at least as large as that from the EUV, if the optical and X-ray emission originate in the same emission region. The variable scattered spectrum from the IR photons contribute 25 and 8 per cent of the optical *B* band flux in the X-ray high- and low-state spectra, respectively. The only way for there to be large variability in the X-rays and not in the *B* band is for the optical spectrum to originate from a different emission region. Since the observed energy densities in the IR/optical band and in the EUV are approximately equal (Fig. 6), we require the size of the IR/optical source to be at least 7 times larger than that of the X-ray source in order that the energy density of the IR/optical photons in the X-ray source is 1/50 of that due to the EUV bump. The requirement on the size ratio is increased to a factor of 10–20 if we use the total variability shown in Fig. 7, i.e. a factor of 3 from 1988 May 15.97–16.10.

4.2.2 *Varying photons*

The conclusion of the previous section is unaltered if we assume that the X-ray variability is induced by rapid changes in the EUV bump and not by changes in the number or spectrum of the injected energetic electrons. The final electron distribution in a compact object is determined by the cooling rate of the energetic particles as well as the injection rate, and cannot be assumed *a priori*. An increase in the number of seed photons leads to an increase in the cooling rate, and so to a decrease in the number of electrons at a given energy. Even though relativistic electrons are injected into the source at a constant rate, the electron spectrum varies with the amount of cooling. There is again a variable electron population, which produces a variable flux in the optical from scattered IR photons so the results of the previous section apply. The variable flux in the optical from the scattered IR photons would have been easily observed.

4.3 X-rays produced by an electron population with $\gamma > 30$

As single emission region models involving upscattering of EUV photons by electrons of energy $\gamma < 30$ have been ruled out, we now consider models in which the X-rays are produced by a variable population of highly energetic electrons. The seed photons are then photons or virtual photons of much lower energy than the EUV bump. The observations still rule out a cospatial origin for the IR/optical and X-ray flux, as the amount of *direct* radiation in the optical band from the component producing the varying X-rays is too high.

The normalization of the high-state X-ray spectrum with $\alpha = 0.79$ is such that if it continued unbroken down to the photon seed source energy, then the variability in this spectrum would have been detected in the optical band. In order for this variable component not to be seen, the spectrum must flatten (α decreasing) at an energy between that of the X-ray and the optical bands. However, there is a limit on the size of this break. The flattest X-ray spectrum in all Compton/synchrotron models has an index of $\alpha = 0.5$ if the photons/virtual photons dominate the energy density of the source (see e.g. Rybicki & Lightman 1979). The highly relativistic electrons that are required to scatter the low-energy photons up to X-ray energies cool extremely quickly (on time-scales of $\sim 20\ \gamma_1^{-1}$ s, where $\gamma > 10\ \gamma_1$). Even if no low-energy electrons are initially injected, the rapid cooling means that a low-energy population is soon established. These cooling electrons, the minimum low-energy population, produce a radiation spectrum with an index of $\alpha = 0.5$. The position of the break from $\alpha = 0.79$ to 0.5 must be at energies below 2 keV. It can be restricted still further by assuming that the X-ray power law extends down to 0.2 keV, as was the case for the *EXOSAT* ME and LE observations reported by Lawrence *et al.* (1985). The cooling spectrum follows the X-ray variability and radiates directly into the *B* band, giving it ~ 3 per cent of the observed *B* band flux in the high X-ray state, violating the observed variability limit of 1 per cent. The constraint obtained earlier continues to hold; the IR/optical component of the spectrum from the nucleus must originate from a region which is spatially separate, or much larger than, the X-ray source. Why similar amounts of power are emitted in the IR/optical and X-ray bands remains a puzzle.

5 CONCLUSIONS

We have observed NGC 4051 simultaneously in the IR, optical, UV and X-ray wavebands. In the optical and IR, the limits on the amount of rapid variability (5–240 min) are below 1 and 5 per cent, respectively, while the X-ray flux continually flickered by up to a factor of 2. The ratio of the amplitude of variability in the X-ray and optical bands is at least 50 to one. This rules out all models in which the IR/optical and X-ray emission are produced in the same region. The IR/optical source must be at least an order of magnitude larger than, or completely separate from, the X-ray source. Models of the X-ray continuum spectrum are not required to produce the IR/optical spectrum simultaneously from the same region.

ACKNOWLEDGMENTS

We thank Tim Naylor for useful discussions about the optical data. CD and ACF acknowledge support from the Carnegie Trust and the Royal Society, respectively.

REFERENCES

Arnaud, K. A., Branduardi-Raymont, G., Culhane, J. L., Fabian, A. C., Hazard, C., McGlynn, T. A., Shafer, R. A., Tennant, A. F. & Ward, M. J., 1985. *Mon. Not. R. astr. Soc.*, **217,** 105.

Edelson, R. A. & Malkan, M. A., 1986. *Astrophys. J.*, **308,** 59.

Ghisellini, G., George, I. M. & Done, C., 1989. *Mon. Not. R. astr. Soc.*, **241,** 43P.

Lawrence, A., Giles, A. B., McHardy, I. M. & Cooke, B. A., 1981. *Mon. Not. R. astr. Soc.*, **195,** 149.

Lawrence, A., Watson, M. G., Pounds, K. A. & Elvis, M., 1985. *Mon. Not. R. astr. Soc.*, **217,** 685.

Lawrence, A., Pounds, K. A., Watson, M. G. & Elvis, M. S., 1987. *Nature,* **325,** 694.

Lyutyi, V. M., 1977. *Soviet Astr.*, **21,** 655.

Makino, F., *et al.*, 1987. *Astrophys. J.*, **313,** 662.

Malkan, M. A. & Filippenko, A. V., 1983. *Astrophys. J.*, **275,** 477.

Matsuoka, M., Yamauchi, M., Piro, L. & Murakami, T., 1989. *Astrophys. J.*, submitted.

Penston, M. J., Penston, M. V. & Sandage, A., 1971. *Publs Astr. Soc. Pacif.*, **83,** 783.

Penston, M. V., Penston, M. J., Selmes, R. A., Becklin, E. E. & Neugebauer, G., 1974. *Mon. Not. R. astr. Soc.*, **169,** 357.

Peterson, B. M., Crenshaw, D. M. & Meyers, K. A., 1985. *Astrophys. J.*, **298,** 283.

Rybicki, G. B. & Lightman, A. P., 1979. *Radiative Processes in Astrophysics,* Wiley, New York.

Sanders, D. B., Phinney, E. S., Neugebauer, G., Soifer, B. T. & Matthews, K., 1989. *Astrophys. J.*, in press.

Savage, B. D. & Mathis, J. S., 1979. *Ann. Rev. Astr. Astrophys.*, **17,** 73.

Seaton, M. J., 1979. *Mon. Not. R. astr. Soc.*, **187,** 73P.

Turner, T. J. & Pounds, K. A., 1989. *Mon. Not. R. astr. Soc.*, **240,** 833.

Ward, M., Elvis, M., Fabbiano, G., Carleton, N. P., Willner, S. P. & Lawrence, A., 1987a. *Astrophys. J.*, **315,** 74.

Ward, M., Geballe, T., Smith, M., Wade, R. & Williams, P., 1987b. *Astrophys. J.*, **316,** 138.

Zdziarski, A. A., 1986. *Astrophys. J.*, **305,** 45.